Dalton Transactions

PAPER

View Article Online
View Journal | View Issue

Cite this: *Dalton Trans.*, 2014, **43**, 16745

Sodium thiosulfate-assisted synthesis of NiS_2 nanostructure by using nickel(II)-Salen precursor: optical and magnetic properties†

Raziyeh Akbarzadeh, Hossein Dehghani* and Fatemeh Behnoudnia

A NiS_2 nanostructure with a protective layer of Ni^{2+} and SO_4^{2-} ions around it has been successfully synthesized using the Ni(II)-Salen (Salen = *N*,*N*′-bis(salicylidene)ethylenediamine) complex *via* a simple solvothermal approach in the presence of anhydrous sodium thiosulfate ($Na_2S_2O_3$) as sulfur source and stabilizer. Unexpectedly, no one kind of pure nickel sulfide nanostructure was prepared using the Ni(II)-Salophen complex or some of the simple mono and bidentate Ni(II) complexes as starting materials and the obtained products were a mixture of nickel sulfides. In the photoluminescence spectrum of the prepared NiS_2, two peaks were evident at 400 and 420 nm with emission maxima, and one broad peak with emission minima was located at 800 nm. The as-synthesized NiS_2 nanostructure displays a weak ferromagnetic behaviour at room temperature, which has small remanent magnetization and saturation magnetization compared to bulk NiS_2. These changes might be attributed to the existence of a protective layer of nickel and sulfate ions around the NiS_2 nanostructures that was confirmed by Energy-dispersive X-ray spectroscopy (EDS), Fourier transform infrared (FTIR) and Raman spectroscopy. The prepared nanostructure has been characterized structurally, electrochemically, optically and magnetically by available methods like X-ray powder diffraction (XRD), Scanning electron microscopy (SEM), Transmission electron microscopy (TEM), Energy-dispersive X-ray spectroscopy, Fourier transform infrared and Raman spectroscopy, Cyclic voltammetry (CV), Photoluminescence (PL) spectroscopy and vibrating sample magnetometer (VSM).

Received 25th July 2014,
Accepted 15th September 2014

DOI: 10.1039/c4dt02232g

www.rsc.org/dalton

Introduction

It is known that metal sulfides exhibit interesting electronic properties, and thus have several technological applications. Many unique and interesting properties, in contrast to their bulk species, have been exhibited for this class of materials such as higher luminescence efficiency, superior mechanic toughness, and lowered lasing threshold.[1–3] Among the family of metal sulfides, nickel sulfides, as important inorganic functional materials, have attracted considerable attention because of practical applications, such as paramagnetic–antiferromagnetic (PM–AFM) phase-changing materials, metal–insulators, magnetic resonance imaging, magnetic refrigeration and as possible transformation harden the window glass.[3,4] Many methods have been introduced to synthesize nanomaterials such as hydrothermal synthesis, microwave irradiation, ultrasonic irradiation.[5–8] In particular, the solvothermal method is a convenient method, because using this method the high purity, size- and shape-controlled nickel sulfide nanostructures can be easily formed. Cubic pyrite NiS_2 dodecahedrons and microspheres have been synthesized in ethylenediamine–glycol mixed solvent at 200 °C using $NiCl_2{\cdot}6H_2O$ and sulfur, as precursors, by a solvothermal approach.[9] The thermal stability of the pyrite NiS_2 dodecahedrons has been studied and they can act as an excellent precursors for the synthesis of porous NiO microspheres by calcination in air atmosphere. Nickel sulfides exhibit magnetic phase behavior. For example, Ni_3S_4 has a metallic character and exhibits itinerant electron ferromagnetism. In contrast, NiS_2 is an insulating antiferromagnetic molecule despite the half-filled e_g band and is consequently considered to be a Mott insulator.[10,11] It consists of a very rich phase diagram in magnetic and transport properties.[12,13] NiS_2 has applications as a cathode material in rechargeable lithium batteries, as a counter electrode for dye sensitized solar cells and as a hydrogenation catalyst.[14–17] It is also potentially useful in sensors and IR detectors.[18,19] It has been pointed out that Schiff bases are among the most popular ligands because of their easy formation and rich coordination chemistry with a

Department of Inorganic Chemistry, Faculty of Chemistry, University of Kashan, Kashan, I. R. Iran. E-mail: dehghani@kashanu.ac.ir; Fax: +98 361 591 2397; Tel: +98 361 5591 2386

† Electronic supplementary information (ESI) available: Additional experimental results as discussed in the text (Fig. S1–S3). See DOI: 10.1039/c4dt02232g

large variety of metal ions.[20,21] Considerable research efforts have been devoted for the synthesis of new complexes with transition and main group metal ions.[22,23] Tetradentate Schiff bases, such as H_2Salen and H_2Salophen ligands, have extensive applications in the fields of synthesis and catalysis.[24–26] These types of ligands contain two imine groups and two phenolic oxygen donors. This arrangement of atoms has provided the condition to synthesize square planar metal complexes that very well stabilize transition metal centers. These types of complexes are flexible and can adopt a variety of structures to provide several active site environments allowing different oxidation reactions.[27,28] H_2Salen and H_2Salophen ligands can be bond to various metals to form soluble and luminescent complexes. In contrast to nanomaterials synthesized from inorganic solids, the synthesis of nanostructure metal compounds based on organic-metal complexes, as precursors, appears to be surprisingly scarce. In this work, we adapted a simple solvothermal route for the preparation of NiS_2 nanostructures by the direct reaction of the Ni(II)-Salen complex and $Na_2S_2O_3$ as sulfur source and stabilizer in DMF solvent. For comparison, Ni(II)-Salophen, $NiCl_2{\cdot}6H_2O$, $NiSO_4{\cdot}6H_2O$ and $Ni(CH_3COO)_2{\cdot}4H_2O$ were used in the same conditions. According to the effect of the precursor on the type and purity of the products, an easy synthesis of tetradentate Schiff bases was performed. On the other hand, because of the diversity of nickel sulfides, the interesting finding in our study is the ability of the aliphatic tetradentate Ni(II)-Schiff base complex (Ni(II)-Salen) to synthesize one type of pure nickel sulfide nanostructure, as opposed to the aromatic tetradentate Ni(II)-Schiff base complex (Ni(II)-Salophen) or simple mono and bidentate Ni(II) complexes. A full description of the reaction mechanisms is discussed in this paper.

Experimental

Common reagents such as ethylenediamine, salicylaldehyde, nickel(II) chloride hexahydrate ($NiCl_2{\cdot}6H_2O$), nickel(II) sulfate hexahydrate ($NiSO_4{\cdot}6H_2O$), nickel(II) acetate tetrahydrate ($Ni(CH_3COO)_2{\cdot}4H_2O$), anhydrous sodium thiosulfate ($Na_2S_2O_3$), *N*,*N*-dimethylformamide (DMF) and *N*,*N*-dimethylacetamide (DMA) were procured from Merck and used without further purifications. Absolute ethanol, double distilled water and hexane were used during the preparation of powders. Powder X-ray diffraction (XRD) measurements were performed using a Phillips X' Pert PRO equipped with a Cu Kα source having a scanning range of 0°–80° Bragg's angle. The morphology of the synthesized products was directly observed by a Philips XL-30 ESEM Scanning electron microscope (SEM) equipped with an Energy-dispersive X-ray spectroscopy (EDS). The Transmission electron microscopy (TEM) images were obtained by dispersing the sample in ethanol and placing a drop of dispersion on a carbon coated copper grid in a Zeiss EM10C instrument operating at 80 kV. Fourier transform infrared (FTIR) spectra were recorded with a Magna 550 Nicolet instrument, in the spectral range between 4000 and 400 cm^{-1}, using KBr pellets. The Raman spectrum was measured with a SENTERRA laser Raman spectrometer in the range 200–3500 cm^{-1} at room temperature. The photoluminescence (PL) of the sample was measured on a Hitachi 850 fluorescence spectrophotometer at room temperature. A computerized electrochemistry system (Sama 500 potentiostat (Isfahan, Iran)) was used to investigate the electrochemical behavior of the obtained NiS_2 nanostructure. In addition, magnetic characterization of the nickel sulfide nanostructures was performed to measure their magnetic properties at room temperature by a BHV-55 (Riken, Japan) vibrating sample magnetometer (VSM).

Synthesis of Schiff base ligands

H_2Salen was prepared according to the literature procedure.[29,30] In brief, a solution containing one equivalent of ethylenediamine (50 mmol) in ethanol was slowly added to a stirred solution of the two equivalents of salicylaldehyde (100 mmol) in ethanol. The reaction mixture was refluxed for 1.5 h and the yellow Schiff base ligand precipitated. After cooling, the ligand was filtered and washed with cold ethanol and dried. The Schiff base of H_2Salophen was prepared according to the same procedure, but 1,2-phenylenediamine was used instead of ethylenediamine and the color of product was orange.

Synthesis of the complexes

The complexes presented in Fig. S1a and b† were synthesized as follows: a stirring solution of Ni(II) acetate tetrahydrate (2 mmol) and appropriate equivalents of Schiff base ligand (2 mmol) in 50 ml ethanol were refluxed for 1.5 h. The progress of the reaction was monitored by TLC until the ligand spot disappeared. The mixture was cooled and the obtained solid was filtered, and then washed with cold ethanol, diethyl ether and dried.[30,31]

Preparation of NiS_2 nanostructures

NiS_2 nanostructures were synthesized by the reaction of Ni(II)-Salen complex (0.46 mmol) and $Na_2S_2O_3$ (0.46 mmol) in 15 ml (DMF) solvent. The reaction mixture was stirred, and then transferred into an autoclave (25 ml) and maintained at 150 °C for 15 h. After cooling to room temperature, the black products were filtered and washed several times with double distilled water, absolute ethanol and hexane. Finally, the prepared product was dried in air at 60 °C for 6 h.

Results and discussion

Fig. 1a shows the typical XRD pattern acquired from the NiS_2 nanostructure with a protective layer of Ni^{2+} and SO_4^{2-} ions around it, which was synthesized using Ni(II)-Salen complex and $Na_2S_2O_3$ as starting materials in DMF solvent at 150 °C for 15 h. All the diffraction peaks belong to anorthic (triclinic) NiS_2 (JCPDS 73-0574) with pure crystallinity. No additional peaks corresponding to metallic nickel or any other forms of nickel sulfides were observed in the XRD pattern, indicating

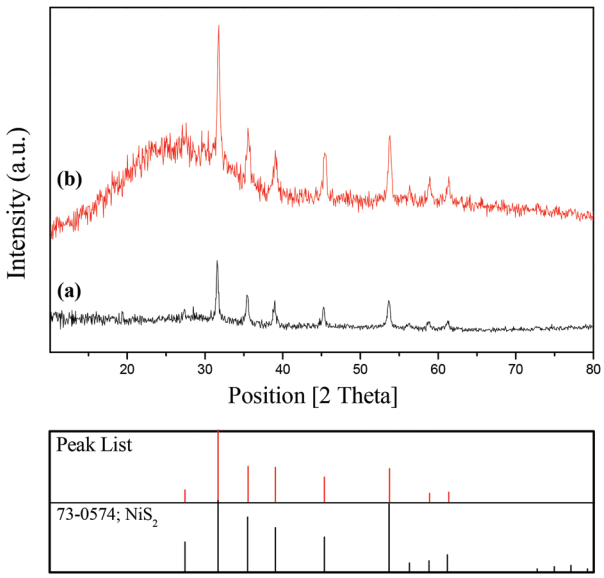

Fig. 1 XRD patterns of the NiS_2 nanostructure synthesized using Ni(II)-Salen complex and $Na_2S_2O_3$ as the starting material for different reaction times (a) 15 h (b) 48 h.

the high purity of the obtained NiS_2. The absence of nickel sulfate peaks indicates the possibility that nickel sulfate is present only as an amorphous phase. As shown in Fig. 1b, it was noticeable that when the reaction time increased to 48 h all the diffraction peaks could also be indexed to anorthic NiS_2 (JCPDS 73-0574). This result proved that a time increment above 15 h has no specific effects on the resultant product and the peaks corresponding to NiS_2 had a high intensity and no additional peaks were observed. The roughness in the baseline of XRD pattern was because of the amorphous silica.

Furthermore, the chemical composition of the prepared sample was determined by EDS analysis. Fig. 2 presents the EDS spectrum of the NiS_2 nanostructure obtained using the Ni(II)-Salen complex and $Na_2S_2O_3$ as the starting materials at 150 °C for 15 h. It can be clearly seen that the as-prepared sample consisted of Ni, S and O. The peaks at 0.9, 7.5 and

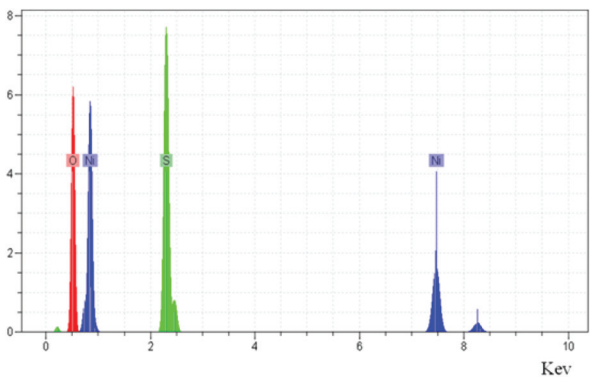

Fig. 2 EDS spectrum of the NiS_2 nanostructure synthesized using Ni(II)-Salen complex and $Na_2S_2O_3$ as the starting materials for a reaction time of 15 h.

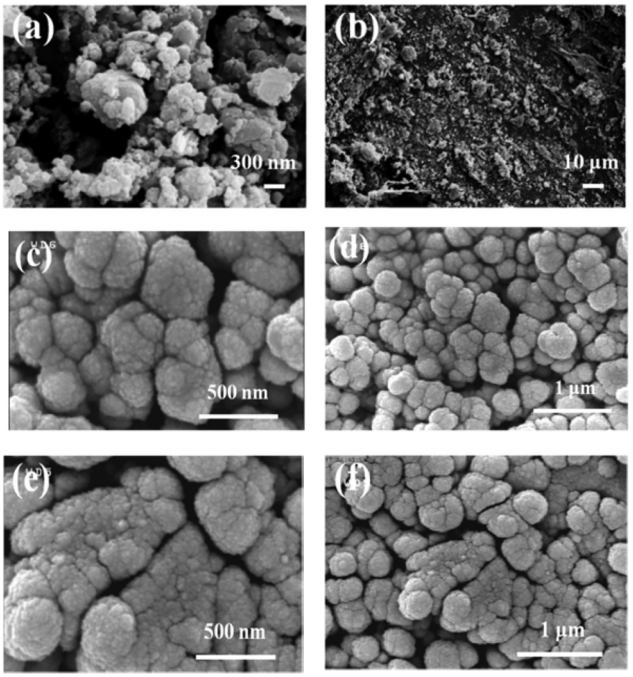

Fig. 3 SEM images of the products synthesized using the Ni(II)-Salen complex, obtained after different reaction times (a, b) 8 h, (c, d) 15 h and (e, f) 48 h.

8.3 keV correspond to nickel, while those at 0.5 and 2.3 keV correspond to oxygen and sulfur, respectively. The sulfur peak is attributed to sulfide in the NiS_2 nanostructure; however, sulfur and oxygen peaks are due to SO_4^{2-} anions around the nanostructures.

Fig. 3 shows the SEM images of the samples obtained by mixing Ni(II)-Salen complex and $Na_2S_2O_3$ for 8 h, 15 h, and 48 h, respectively. It can be seen in Fig. 3a and b that the sample obtained after 8 h has non-uniform nanoparticle morphology with several tens of nanometers in size, which act as the building block units. The product obtained after 15 h has a special structure with an average diameter of about 200 nm, which consists of very small particles that tend to coalesce (Fig. 3c and d). Such special morphology might because of the SO_4^{2-} anions and adsorbed water molecules around the nanostructure. As can be seen in Fig. 3e and f, a similar morphology is observed for the NiS_2 samples obtained by increasing the time to 48 h. From the SEM images of NiS_2 nanostructures, it was observed that the nanostructures were almost uniform in size.

The particle size was evaluated by the Scherrer formula:[5]

$$D = \frac{K\lambda}{\beta \cos\theta}$$

where D is the average dimension of crystallites; K is the Scherrer constant, (K = 0.89); λ is the wavelength of the Cu Kα_1 radiation (0.1541 nm), θ is the Bragg angle of the peak and β is the corrected half-width of the diffraction peak. The average crystalline size of the NiS_2 synthesized after 15 h was calculated to be approximately 28.6 nm using this formula.

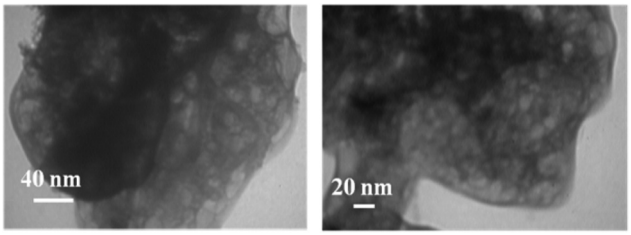

Fig. 4 TEM images of the NiS_2 nanostructure synthesized using Ni(II)-Salen complex and $Na_2S_2O_3$ as the starting materials for a reaction time of 15 h.

Because the SEM images of the NiS_2 nanostructure typically show the aggregation of particles, supplementary TEM measurements were carried out. Fig. 4 shows the TEM images of the product obtained after 15 h of reaction. It is noticeable that TEM images establish that most of the very small NiS_2 particles (<20 nm) tend to coalesce and the nanoparticles formed by the interconnected crystallites might be due to the layer of SO_4^{2-} anions, which act as stabilizer and adsorbed water molecules, which surround the NiS_2 particles.

The FTIR spectrum of the prepared NiS_2 nanostructure after a reaction time of 15 h is shown in Fig. 5a and it contains a broad peak for asymmetric and symmetric stretching vibrations of the adsorbed water molecules at 3429 cm^{-1} and a bending vibration band for water at 1627 cm^{-1}.[32] The absorption bands at 1107 cm^{-1} and 613 cm^{-1} can be attributed to vibrations of SO_4^{2-} ν(S–O) and ν(O–S–O), respectively.[33] As expected, the FTIR spectrum confirmed the presence of sulfate anions directed toward water around the as-prepared nanostructure. For further confirmation and characterization, the Raman spectrum of the typical NiS_2 nanostructure obtained after a reaction time of 15 h with an average diameter of roughly 200 nm was also carried out at room temperature, as shown in Fig. 5b. The peaks at 279, 306, 410, 557 and 676 cm^{-1} are related to NiS_2 and the peaks at 968, 1152, 1301 and 1562 cm^{-1} correspond to sulfate anions around the nanostructure. In addition, the broad peak between 1500–1700 cm^{-1} and the small peak at 3253 cm^{-1}, could be attributed to the bending and symmetric stretching vibration of the adsorbed water molecules.[34] The Raman peaks of NiS_2 nanostructures with no protective layer, which were synthesized by Wang *et al.*, appeared at 210, 262, 518 cm^{-1}.[35] The observed vibrational modes resulting from the spectrum are also shown in Table 1. For comparison, the literature data are also listed in the table.[4,33,36] As can be seen from the data shown in Fig. 5b and Table 1, the Raman modes of the as-prepared NiS_2 nanostructure, are significantly shifted towards a higher wavenumber (blue shift) compared to NiS_2 powders previously reported.[4,33,35] Therefore, the reason for these changes in Raman shifts is probably because of the small size of the particles in the special structural morphology of NiS_2 and the shifts can be mainly attributed to the existence of the protective layer of Ni^{2+} and SO_4^{2-} ions and adsorbed water molecules around the nanostructures and to intermolecular interactions. Thus, the Raman spectrum obtained at room temperature identified that the product was a NiS_2 nanostructure along with a stabilizer layer of sulfate anions and adsorbed water molecules around it.

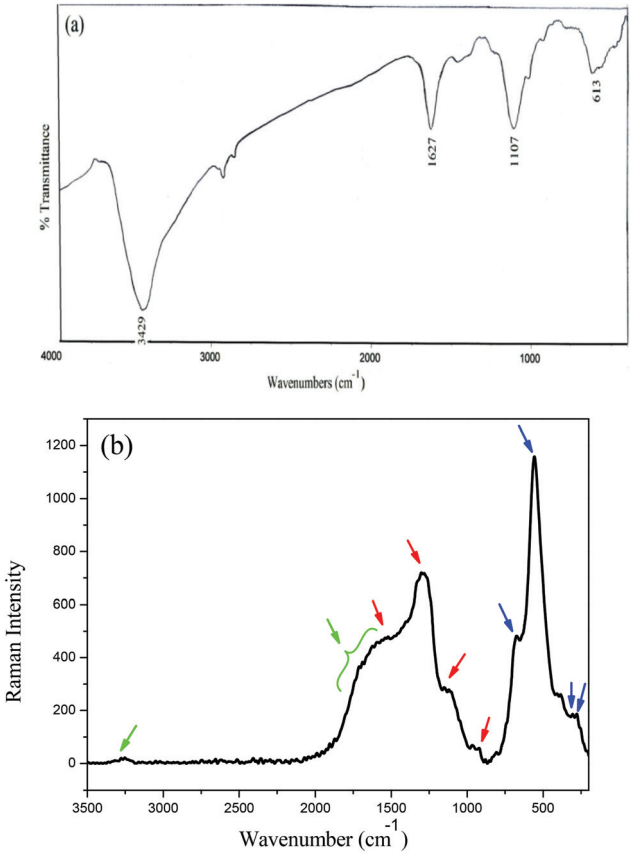

Fig. 5 (a) FTIR and (b) Raman spectra of the as-prepared NiS_2 nanostructure after a reaction time of 15 h (The Raman peaks of NiS_2, sulfate ions and adsorbed water molecules are shown as blue, red and green arrows, respectively).

Table 1 List of the vibrational frequencies (cm^{-1}) derived from the spectrum shown in Fig. 4b

NiS_2 powder peak position (cm^{-1})[4]	Prepared NiS_2 nanostructure peak position (cm^{-1})	$NiSO_4$ powder peak position (cm^{-1})[33,36]
235	279	
274	308	
373	410	
515	557	
562	676	
	968	970
	1152	1075
	1301	1176
	1562	1211

To find the different effects of aliphatic and aromatic tetradentate Ni(II)-Schiff base complexes when used as precursors, the reaction was carried out using similar procedure by the substitution of Ni(II)-Salophen complex, which was an aromatic tetradentate Ni(II)-Schiff base complex with the Ni(II)-

Table 2 Experimental parameters for the products synthesized using the Ni(II)-Salophen complex at 180 °C

Sample	Concentration of Ni(II) comp. (mmol)	Ni(II) comp.: $Na_2S_2O_3$ (mole ratio)	Time/h	Solvent
S1	0.46	1 : 1	8	DMF
S2	0.46	1 : 1	15	DMF
S3	0.46	1 : 1	24	DMF
S4	0.46	1 : 1	8	DMA
S5	0.46	1 : 1	15	DMA
S6	0.46	1 : 1	24	DMA
S7	0.46	3 : 4	15	DMA
S8	0.80	1 : 1	15	DMF

Salen complex. Table 2 shows applied synthesis conditions such as solvent, time, concentration and mole ratio of the starting materials, for the preparation of nickel sulfide nanostructures using the Ni(II)-Salophen complex. It should be noticed that no products are obtain at 150 °C in the presence of Ni(II)-Salophen complex and the reaction requires higher temperature of about 180 °C. This was because of the resonance effect in the H_2Salophen structure, which made the nickel center more stable than in the H_2Salen structure.

Fig. 6a presents a typical XRD pattern of the sample obtained by mixing the Ni(II)-Salophen complex and $Na_2S_2O_3$ in 15 ml DMF at 180 °C for 15 h (S2). The reflection peaks can be indexed as the mixture of cubic Ni_3S_4 (JCPDS 76-1813), rhombohedral NiS (JCPDS 86-2280) and hexagonal NiS (JCPDS 75-0613). By changing the solvent to DMA and fixing other reaction conditions (S5), the XRD pattern indicates that the product is the mixture of cubic Ni_3S_4 (JCPDS 76-1813), rhombohedral NiS (JCPDS 86-2280) and a trace of hexagonal NiS (JCPDS 75-0613), as can be seen in Fig. 6b. Increasing the mole ratio of Ni(II)-Salophen complex : $Na_2S_2O_3$ from 1 : 1 to 3 : 4 in 15 ml DMA (S7) displays that the sample was also composed of cubic Ni_3S_4 (JCPDS 76-1813), rhombohedral NiS (JCPDS 86-2280) and a trace of hexagonal NiS (JCPDS 75-0613), and did not show any remarkable changes. The corresponding XRD pattern is shown in Fig. 6c. Therefore, increasing the amount of $Na_2S_2O_3$ is not effective in the preparation of a pure nickel sulfide. As shown in Fig. 6d, if the concentration of Ni(II)-Salophen complex increased to 0.80 mmol (S8), in addition the peaks associated to Ni_3S_4 (JCPDS 76-1813), the peaks related to rhombohedral NiS (JCPDS 86-2280) and hexagonal NiS (JCPDS 75-0613) appeared, but with a low intensity. However, it was concluded that no pure nickel sulfide nanostructures were produced by using the Ni(II)-Salophen complex as the precursor under these conditions.

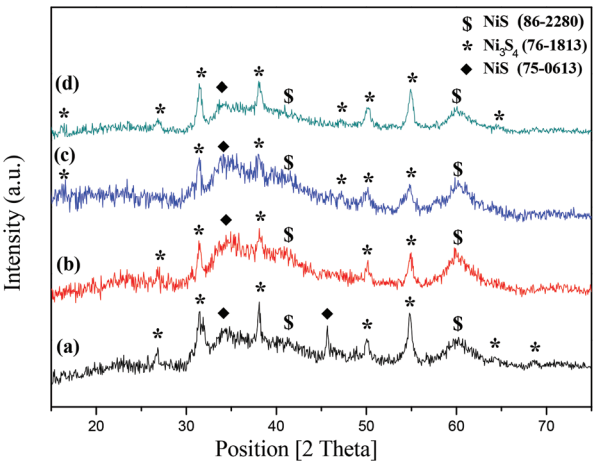

Fig. 6 XRD patterns of the products synthesized by using the Ni(II)-Salophen complex and $Na_2S_2O_3$ as the starting materials under different conditions (a) S2 (b) S5 (c) S7 (d) S8.

The SEM images of the samples obtained by mixing the Ni(II)-Salophen complex and $Na_2S_2O_3$ in 15 ml DMF at 180 °C for 8 h (S1), 15 h (S2) and 24 h (S3) are shown in Fig. S2a–c,† respectively. Fig. S2d–f,† are related to the SEM images of the prepared Ni_3S_4 in DMA, while other reaction conditions were fixed, *i.e.* (S4), (S5) and (S6). From the image, it can be observed that the products have an erratic and non-uniform surface (except for the product obtained after 15 h of reaction time in DMA (Fig. S2e†) that has a more uniform and homogeneous particle size distribution in comparison to samples obtained after 8 h and 24 h). For these reaction times, the nanoparticles agglomerated. Fig. 7 presents the SEM images of the sample obtained by mixing 0.8 mmol Ni(II)-Salophen complex in 15 ml DMF at 180 °C for 15 h (S8) in which porous and homogenous structures composed of nanosheets are observed.

Surprisingly, from the FTIR spectrum related to the sample obtained by mixing 0.8 mmol Ni(II)-Salophen complex at 180 °C for 15 h (S8), in Fig. S3,† the bands at 1120 cm^{-1} and 614 cm^{-1} confirms the existence of sulfate anions, and the two remaining bands at 3427 cm^{-1} and 1612 cm^{-1} agree with the adsorbed water molecules, around the as-synthesized products.

If we fix all the reaction conditions, but change the Ni(II)-Salen complex to $NiCl_2{\cdot}6H_2O$, $NiSO_4{\cdot}6H_2O$ or ($Ni(CH_3COO)_2{\cdot}4H_2O$), the products are a mixture of NiS and Ni_3S_4 and no one type of pure nickel sulfide nanostructures are obtained. Therefore, as can be seen in Fig. 8, all the reflection peaks can be indexed to rhombohedral NiS (JCPDS 86-2280) and cubic Ni_3S_4 (JCPDS 76-1813). Furthermore, a trace of hexagonal NiS (JCPDS 75-0613) appeared in Fig. 8a and b

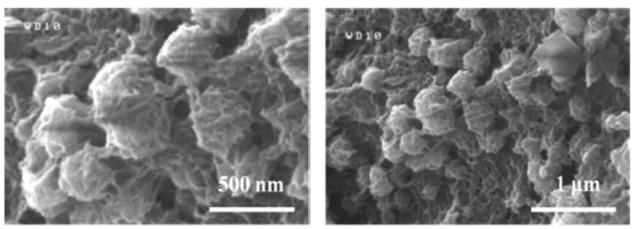

Fig. 7 SEM images of the sample synthesized by using 0.80 mmol of Ni(II)-Salophen complex (S8).

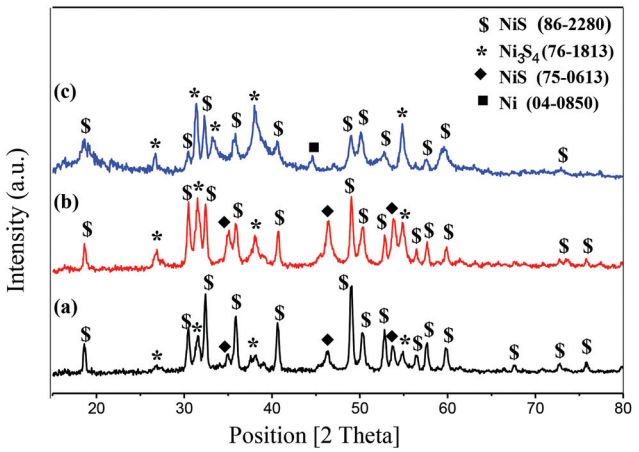

Fig. 8 XRD patterns of the products synthesized at 150 °C for 48 h using (a) nickel chloride (b) nickel sulfate (c) nickel acetate, as the starting material.

and a trace of cubic Ni (JCPDS 04-0850) is also observed in Fig. 8c.

On the basis of the results described above, we propose the possible growth mechanisms of different products. In the reaction between tetradentate Ni(II)-Schiff base complexes and $Na_2S_2O_3$ in the DMF solvent, two solvent molecules occupy the empty sites of square planar Ni(II)-Salen and Ni(II)-Salophen complexes at the early stage of the reaction. Moreover, $Na_2S_2O_3$ decomposes to Na_2SO_3 and S upon heating, and then the Na_2SO_3 is further converted to Na_2S and Na_2SO_4 through a disproportionation process. In this reaction process, first, NiS was obtained, and then in the reaction with sulfur, it was transformed to NiS_2. The type of nickel sulfides obtained strongly dependent on the starting materials. Using Ni(II)-Salen as the precursor, at 150 °C, results in pure NiS_2 nanostructure. On the basis of our previous report,[37] it is likely that the obtained Ni^{2+} and SO_4^{2-} ions and adsorbed water molecules act as the stabilizing agents for the nanostructures and create a rigid protective layer around the nanostructures, which could promote shape control on the growth of NiS_2 nanostructures. However, in the presence of the Ni(II)-Salophen complex, as mentioned above, no product was obtained at 150 °C and by increasing the temperature to 180 °C, a mixture of Ni_3S_4 and two types of NiS was obtained. These changes may be attributed to the decomposition of H_2Salophen to starting materials, at this temperature, because the phenyl ring in the formed 1,2 phenylenediamine was oxidized and caused the reduction of Ni^{2+} to Ni. Therefore, Ni_3S_4 nanostructures were produced by combining Ni and two equivalents of NiS_2. It is noteworthy that during the reaction path using the Ni(II)-Salen complex, nickel production did not occur and Ni_3S_4 was not observed in the final product. Another method to prepare Ni_3S_4 is by combining NiS_2 and two equivalents of NiS. Because the reaction using the Ni(II)-Salen complex produced NiS and NiS_2, but did not produce any Ni_3S_4 so this method was not suitable for our proposed mechanism. Consequently, the reaction processes can be described as follows:

(a) The product synthesized from the Ni(II)-Salen complex:

$$\mathrm{Ni(Salen)} + 2\mathrm{DMF} \rightarrow [\mathrm{Ni(Salen)(DMF)_2}] \quad (1)$$

$$[\mathrm{Ni(Salen)(DMF)_2}] + 4\mathrm{S_2O_3}^{2-} \rightarrow \mathrm{NiS}\downarrow + 3\mathrm{SO_4}^{2-} + 4\mathrm{S} + \mathrm{Salen}^{2-} + 2\mathrm{DMF} \quad (2)$$

$$\mathrm{NiS} + \mathrm{S} \rightarrow \mathrm{NiS_2} \quad (3)$$

(b) The products synthesized from the Ni(II)-Salophen complex:

$$\mathrm{Ni(Salophen)} + 2\mathrm{DMF} \rightarrow [\mathrm{Ni(Salophen)(DMF)_2}] \quad (4)$$

$$[\mathrm{Ni(Salophen)(DMF)_2}] + 4\mathrm{S_2O_3}^{2-} \rightarrow \mathrm{NiS}\downarrow + 3\mathrm{SO_4}^{2-} + 4\mathrm{S} + \mathrm{Salophen}^{2-} + 2\mathrm{DMF} \quad (5)$$

$$\mathrm{Salophen}^{2-} + 2\mathrm{H_2O} \rightleftharpoons \mathrm{H_2\text{-}Salophen} + 2\mathrm{OH}^- \quad (6)$$

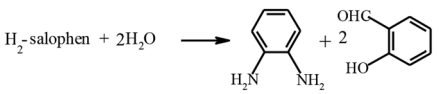

(7)

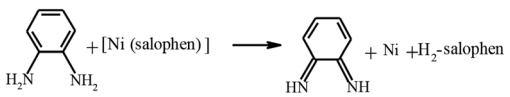

(8)

$$\mathrm{Ni} + 2\mathrm{NiS_2} \rightarrow \mathrm{Ni_3S_4} \quad (9)$$

We suppose that the formation mechanism of the nickel sulfides from $NiCl_2{\cdot}6H_2O$, $NiSO_4{\cdot}6H_2O$ or $Ni(CH_3COO)_2{\cdot}4H_2O$ complexes with $Na_2S_2O_3$ are similar to Ni(II)-Salen or Salophen complexes, but the required nickel for the production of Ni_3S_4 is obtained in the DMF solvent that has a larger tendency for the reduction of Ni^{2+}, which can be explained in equations as follows:[38,39]

$$\mathrm{Ni^{2+}} + \mathrm{HCONMe_2} + \mathrm{H_2O} \rightarrow \mathrm{Ni} + \mathrm{Me_2NCOOH} + 2\mathrm{H}^+ \quad (10)$$

$$\mathrm{Me_2NCOOH} \rightarrow \mathrm{CO_2} + \mathrm{Me_2NH} \quad (11)$$

It was noticeable that using tetradentate Ni(II)-Schiff base complexes, the reduction of Ni^{2+} in the DMF solvent was impossible because the square planar structure of these complexes stabilize the central nickel(II) ion very well. According to these data, the schematic synthetic process for the preparation of nickel sulfide compounds is shown in Fig. 9.

The electrochemical behavior of the NiS_2 nanostructure obtained after a reaction time of 15 h was investigated using cyclic voltammetric in a potential range from 0.0 to 0.6 V using different scan rates (5, 10, 20 and 30 mV s^{-1}) at room temperature and in a 3 M KOH aqueous solution, as shown in Fig. 10. A conventional three-electrode cell was used with a platinum wire as counter electrode, an Ag/AgCl as the reference electrode and a working electrode, which was prepared by dropping an ultrasonically redispersed NiS_2 nanostructure in pure ethanol onto the glassy carbon electrode (2 mm diameter). As seen in Fig. 10, under the influence of applied voltage and with a 5 mV s^{-1} scan rate, a broad oxidation peak around 0.35 V and

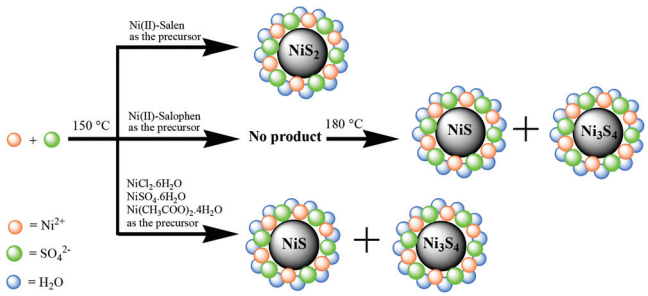

Fig. 9 Schematic diagram illustrating the formation of nickel sulfide compounds.

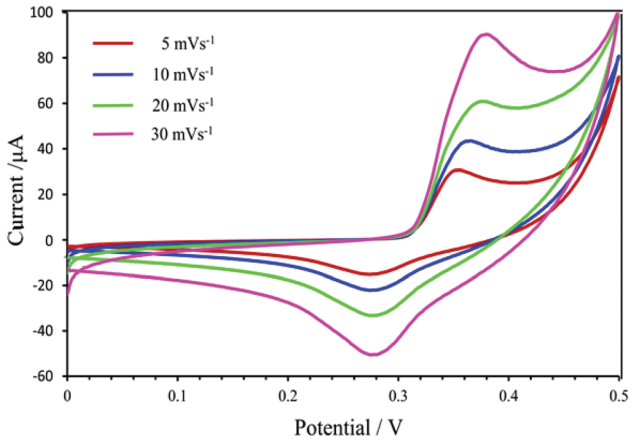

Fig. 10 Cyclic voltammetry of the as-prepared NiS_2 nanostructure after a reaction time of 15 h within a 0.0 to 0.6 V range at different scan rates (5, 10, 20 and 30 mV s^{-1}) at room temperature and in 3 M KOH electrolyte.

a reduction peak at about 0.28 V were observed, which were associated with the oxidation of Ni^{2+} to Ni^{3+} and with the subsequent reduction of Ni^{3+} to Ni^{2+}, respectively. Moreover, the figure shows that the current intensity and potential of the redox peaks are increased by increasing the scanning rate.

Fig. 11 shows the room temperature fluorescence spectra of the NiS_2 nanostructure prepared for 15 h, excited at 325 nm. There is a broad emission for the NiS_2 nanostructure in which the top of the emission peak is separated into two peaks located, respectively, at 400 and 420 nm. The separated peaks might be attributed to the presence of structural defects within the sample due to electronic transitions. A second broad PL emission band with very low intensity, more clearly shown in inset picture of Fig. 11, was observed in the near IR region (about 800 nm). The observed emissions can then be related to the intra-band transitions that occur on the NiS_2 band structure during excitation. Linganiso *et al.* proposed that the NiS_2 luminescence characterized at wavelengths of 400 and 420 nm could result from the de-excitation between S (3p) levels and Ni (3d) levels, whereas those features around 800 nm could be attributed to the de-excitations from either

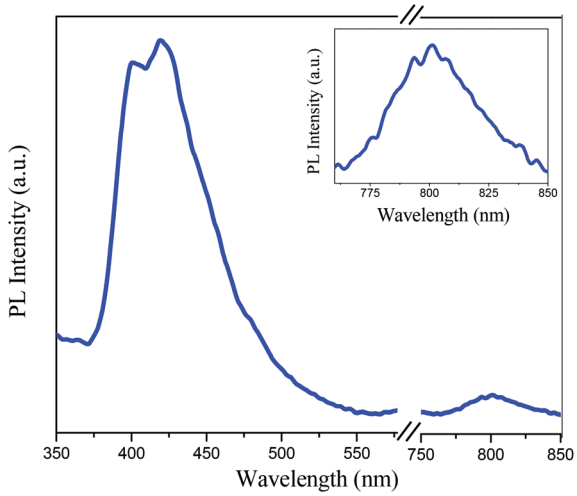

Fig. 11 Photoluminescence spectrum of the as-prepared NiS_2 nanostructure, obtained after a reaction time of 15 h, dispersed in methanol. The inset shows the clearer broad peak in the near IR region.

S (3s, 3p) or Ni (3d) levels down to the Ni–S hybridization levels.[40]

The magnetic property of NiS_2 belongs to a large system of pyrite-type materials that exhibit antiferromagnetic properties.[41] In 1961, Neel *et al.* proposed that fine particles of an antiferromagnetic material should exhibit magnetic properties such as superparamagnetism and weak ferromagnetism.[42] The magnetic hysteresis loop of the NiS_2 nanostructure synthesized after a reaction time of 15 h, shown in Fig. 12, presents a week ferromagnetic behavior. This reveals that the as-prepared NiS_2 nanostructures have small remanent magnetization, saturation magnetization and great coercivity (H_c = 123 Oe), compared to bulk NiS_2 (H_c = 78 Oe) and similar to the values of NiS_2 nanostructures without any protective layer, a decrease in the remanent magnetization and saturation magnetization was observed (M_r = 0.025 emu g^{-1} and M_s = 0.292 emu g^{-1}).[35]

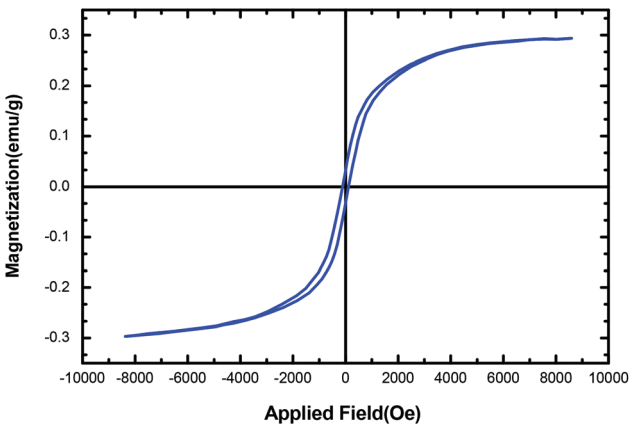

Fig. 12 A magnetization–magnetic field (M–H) plot at room temperature of the as-prepared NiS_2 nanostructure after a reaction time of 15 h.

According to the previous report,[37] the reason for these changes may be the size effect and could be mainly attributed to the presence of the protective layer on the NiS_2 nanostructure.[37,43]

Conclusions

Although there have been numerous studies on the NiS_2 nanostructures precipitation using sodium thiosulphate as a sulfur source, this study focus on the use of sodium thiosulfate as both the sulfur source and the stabilizer to produce a new type of the NiS_2 nanostructures with diverse chemical, optical and magnetic properties. In this work, NiS_2 nanostructures have been successfully prepared *via* a facile solvothermal method using the Ni(II)-Salen complex and $Na_2S_2O_3$ in DMF solvent. The key insights obtained from the our study are that the pure NiS_2 nanostructure can be synthesized from the precursor Ni(II)-Salen complex, which is an aliphatic tetradentate Ni(II)-Schiff base complex, but it is difficult to obtain a pure phase of nickel sulfides using an aromatic tetradentate Ni(II)-Schiff base complex, such as the Ni(II)-Salophen complex or simple mono and bidentate Ni(II) complexes, such as $NiCl_2{\cdot}6H_2O$, $NiSO_4{\cdot}6H_2O$ and $Ni(CH_3COO)_2{\cdot}4H_2O$ complexes, under our reaction conditions. It can be pointed out that the existence of Ni^{2+} and SO_4^{2-} ions and adsorbed water molecules, thereby create a protective layer around the NiS_2 nanostructure, which has been assessed by EDS, FTIR and Raman spectroscopy, in the current study, playing a crucial role in the chemical and magnetic properties of the NiS_2 nanostructure. A corollary to this rule is that the saturation magnetization (M_s) and remanent magnetization (M_r) of the as-prepared NiS_2 nanostructure were found to be 0.292 emu g^{-1} and 0.025 emu g^{-1}, respectively, when compared to bulk NiS_2 and NiS_2 nanostructures without any protective layer, resulted in lower values of M_s and M_r. Additionally, it was interesting that a time increment higher than 15 h did not structurally and morphologically affect the nanostructure. On the basis of these calculations, the choice of the Ni(II)-Salen complex and $Na_2S_2O_3$ as starting materials is critical for preparing the target product and the synthetic strategy might lead the way for the preparation of other inorganic nanomaterials having different properties and morphologies, by using such precursors.

The authors are thankful to the University of Kashan for supporting this work by grant no. 159183/20.

Notes and references

1 Y. N. Xia, P. D. Yang, Y. G. Sun, Y. Y. Wu, B. Mayers, B. Gates, Y. D. Yin, F. Kim and Y. Q. Yan, *Adv. Mater.*, 2003, **125**, 353.
2 J. Hu, T. W. Odom and C. M. Lieber, *Acc. Chem. Res.*, 1999, **32**, 435.
3 S. Nagaveena and C. K. Mahadevan, *J. Alloys Compd.*, 2014, **582**, 447.
4 X. F. Zhou, L. Lin, W. Wang and S. Y. Wang, *J. Cryst. Growth*, 2011, **314**, 302.
5 W. Dong, L. An, X. Wang, B. Li, B. Chen and W. Tang, *J. Alloys Compd.*, 2011, **509**, 2170.
6 W. Zhang, L. Xu, K. Tang, F. Li and Y. Qian, *Eur. J. Inorg. Chem.*, 2005, **2005**, 653.
7 H. Pang, C. Wei, X. Li, G. Li, Y. Ma, S. Li, J. Chen and J. Zhang, *Sci. Rep.*, 2014, **4**, 3577.
8 N. Chen, J. H. Zeng, F. Q. Li, W. Q. Zhang and Y. T. Qian, *J. Cryst. Growth*, 2002, **235**, 505.
9 S. L. Yang, H. B. Yao, M. R. Gao and S. H. Yu, *CrystEngComm*, 2009, **11**, 1383.
10 K. D. M. Rao, T. Bhuvana, B. Radha, N. Kurra and N. S. Vidhyadhiraja, *J. Phys. Chem. C*, 2011, **115**, 10462.
11 P. G. Niklowitz, P. L. Alireza, M. J. Steiner, G. G. Lonzarich, D. Braithwaite, G. Knebel, J. Flouquet and J. A. Wilson, *Phys. Rev. B: Condens. Matter*, 2008, **77**, 115135.
12 G. Krill, P. Panissod, M. F. Lapierre, F. Gautier and C. Robert, *J. Phys.*, 1976, **37**, 23.
13 T. Thio and J. W. Bennett, *Phys. Rev. B: Condens. Matter*, 1995, **52**, 3555.
14 G. Andersen and P. Kofstad, *Oxid. Met.*, 1995, **43**, 173.
15 H. S. Jarret, W. H. Cloud, R. J. Bouchard, S. R. Butler, C. G. Frederick and J. L. Gillison, *Phys. Rev. Lett.*, 1968, **21**, 617.
16 H. M. Mulmudi, S. K. Batabyal, M. Rao, R. R. Pranhakar, N. Mathews, Y. M. Lam and S. G. Mhaisalkar, *Phys. Chem. Chem. Phys.*, 2011, **13**, 19307.
17 S. T. Oyama, *J. Catal.*, 2003, **216**, 343.
18 R. S. Mane and C. D. Lokhande, *Mater. Chem. Phys.*, 2000, **65**, 1.
19 S. Leitz, G. Hodes, R. Tenne and J. Manassen, *Nature*, 1987, **326**, 863.
20 P. A. Vigato and S. Tamburrini, *Coord. Chem. Rev.*, 2004, **248**, 1717.
21 D. A. Atwood, *Coord. Chem. Rev.*, 1997, **165**, 267.
22 W. H. Leung, E. Y. Y. Chan, E. K. F. Chow, I. D. Williams and S. M. Peng, *J. Chem. Soc., Dalton Trans.*, 1996, 1229.
23 D. A. Atwood and M. J. Harvey, *Chem. Rev.*, 2001, **101**, 37.
24 M. Palucki, G. J. Mc Cormick and E. N. Jacobsen, *Tetrahedron Lett.*, 1995, **36**, 5457.
25 T. Yamada, K. Imagawa, T. Nagata and T. Mukaiyama, *Bull. Chem. Soc. Jpn.*, 1994, **67**, 2248.
26 W. Adam, J. Jeco, A. Levai, C. Nemes, T. Patonay and P. Sebok, *Tetrahedron Lett.*, 1995, **36**, 3669.
27 B. Ortiz and S. M. Park, *Bull. Korean Chem. Soc.*, 2000, **21**, 405.
28 K. Yamamoto, K. Oyaizu and E. Tsuchida, *J. Am. Chem. Soc.*, 1996, **188**, 12665.
29 S. L. Barnholtz, J. D. Lydon, G. Huang, M. Venkatesh, C. L. Barnes, A. R. Ketring and S. S. Jurisson, *Inorg. Chem.*, 2001, **40**, 972.
30 L. F. Lindoy, W. E. Moody and D. Taylor, *Inorg. Chem.*, 1977, **16**, 1962.
31 M. Sonmez, M. R. Bayram and M. Celebi, *J. Coord. Chem.*, 2009, **62**, 2728.

32 P. Jeevanandam, Y. Koltypin and A. Gedanken, *Nano Lett.*, 2001, **1**, 263.
33 K. Nakamoto, *Infrared Spectra of Inorganic and Coordination Compounds*, John Wiley, New York, 1997.
34 Q. Sun, *Vib. Spectrosc.*, 2009, **51**, 213.
35 W. Wang, S. Y. Wang, Y. L. Gao, K. Y. Wang and M. Liu, *Mater. Sci. Eng. B*, 2006, **133**, 167.
36 E. Avzianova and S. D. Brooks, *J. Aerosol Sci.*, 2014, **67**, 207.
37 R. Akbarzadeh and H. Dehghani, *Dalton Trans.*, 2014, **43**, 5474.
38 D. Ajloo, B. Yoonesi and A. Soleymanpour, *Int. J. Electrochem. Sci.*, 2010, **5**, 459.
39 I. Pastoriza-Santos and L. M. Liz-Marzan, *Pure Appl. Chem.*, 2000, **72**, 83.
40 E. C. Linganiso, S. D. Mhlanga, N. J. Coville and B. W. Mwakikunga, *J. Alloys Compd.*, 2013, **552**, 345.
41 M. Matsuura, Y. Endoh, H. Hiraka, K. Yamada, A. S. Mishchenko, N. Nagaosa and I. V. Solovyev, *Phys. Rev. B: Condens. Matter*, 2003, **68**, 094409.
42 *Low Temp. Phys.*, ed. L. Neel, C. Dewitt, B. Dreyfus and P. D. De Gennes, Gordon and Beach, New York, 1962, p. 413.
43 X. H. Chen, H. T. Zhang, C. H. Wang, X. G. Luo and P. H. Li, *Appl. Phys. Lett.*, 2002, **81**, 4419.